Biological Conservation 233 (2019) 109–117

Contents lists available at ScienceDirect

Biological Conservation

journal homepage: www.elsevier.com/locate/biocon

Detecting 'poachers' with drones: Factors influencing the probability of detection with TIR and RGB imaging in miombo woodlands, Tanzania

Leonard Hambrecht[a,*], Richard P. Brown[a], Alex K. Piel[a], Serge A. Wich[a,b]

[a] School of Natural Sciences and Psychology, Liverpool John Moores University, UK
[b] Institute for Biodiversity and Ecosystem Dynamics, University of Amsterdam, Amsterdam, the Netherlands

ARTICLE INFO

Keywords:
UAV
Drone
Thermal
TIR
RGB
Comparison
Contrast
Distance
Centerline
Poachers
People
Time of day
Poaching
Conservation
Canopy
Density

ABSTRACT

Conservation biologists increasingly employ drones to reduce poaching of animals. However, there are no published studies on the probability of detecting poachers and the factors influencing detection. In an experimental setting with voluntary subjects, we evaluated the influence of various factors on poacher detection probability: camera (visual spectrum: RGB and thermal infrared: TIR), density of canopy cover, subject distance from the image centreline, subject contrast against the background, altitude of the drone and image analyst. We manually analysed the footage and marked all recorded subject detections. A multilevel model was used to analyse the TIR image data and a general linear model approach was used for the RGB image data. We found that the TIR camera had a higher detection probability than the RGB camera. Detection probability in TIR images was significantly influenced by canopy density, subject distance from the centreline and the analyst. Detection probability in RGB images was significantly influenced by canopy density, subject contrast against the background, altitude and the analyst. Overall, our findings indicate that TIR cameras improve human detection, particularly at cooler times of the day, but this is significantly hampered by thick vegetation cover. The effects of diminished detection with increased distance from the image centreline can be improved by increasing the overlap between images although this requires more flights over a specific area. Analyst experience also contributed to increased detection probability, but this might cease being a problem following the development of automated detection using machine learning.

1. Introduction

Poaching, the unlawful harvest of wildlife products, supports illegal global wildlife trade and is a major conservation issue due to its impact on species extinctions. The demand for illegal wildlife products has risen in the few last years with 7000 species recorded as having been trafficked (Lawson and Vines, 2014; United Nations Office on Drugs and Crime, 2016). This results in the decline of threatened species, as well as rise in international security threats and economic losses (Balazs, 2016; Becker et al., 2013; Chapron et al., 2008; Liberg et al., 2012; Naidoo et al., 2016; United Nations Office on Drugs and Crime, 2016). Wildlife enforcement officers and conservationists try to fight poaching using a variety of methods, such as reducing demand in key areas such as Asia, implementing community conservation areas, deploying ranger patrols in protected areas, strengthening wildlife laws, dehorning rhinos and implementing new technologies such as DNA mapping, mobile biological sensors and drones (Dinerstein et al., 2017; Lunstrum, 2014; Mukwazvure and Magadza, 2014). Drones are a cost-effective and flexible tool that can be used in the field to monitor protected habitat and gather intelligence on wildlife crime activities (Koh and Wich, 2012; Linchant et al., 2015; World Bank, 2018). This intelligence includes the detection of poachers in the field (Air Shepherd, 2017; Mulero-Pázmány et al., 2014; Smart Parks, 2018).

There are several key safety, technical and practical differences between the use of drones for detecting poachers and the more traditional use of manned aircrafts. Most importantly, the latter pose a higher risk to the operator as poachers can deploy powerful weapons. In contrast, drones allow detection while simultaneously minimizing confrontations with poachers (Baggaley, 2017; Parveen, 2016). Secondly, manned aircraft require an on-board observer, while drones can use a variety of sensors to record still and moving images that either need to be viewed as a live stream or analysed after the flight. Additional advantages of using drones include their cost-effectiveness, the fact that they do not require a runway and that they can be programmed to follow precisely a predefined path (Kakaes et al., 2015). Furthermore, drones have been found to be able deliver more accurate

* Corresponding author at: Haydnstrasse 42, 40593 Düsseldorf, Germany.
E-mail address: lennyhambrecht@pm.me (L. Hambrecht).

https://doi.org/10.1016/j.biocon.2019.02.017
Received 28 October 2018; Received in revised form 3 February 2019; Accepted 13 February 2019

animal count data than traditional ground-based surveys (Hodgson et al., 2018).

Although their deployments in anti-poaching efforts are promising, there are no studies that have explicitly investigated the factors that determine detection probability in this specific context. However, it is important to do so for several reasons, including the optimization of flight patterns to improve detection and identify the environmental conditions under which poachers are likely to be missed during drone missions. Fixed wing drones are the preferred tool for anti-poaching operations because of their long flight duration and extended range (Mulero-Pázmány et al., 2014; Olivares-Mendez et al., 2015).

There are various factors that affect the probability of detecting animals – and potentially humans – including body size, position of the sun, distance from the transect, group density, target contrast, terrain ruggedness, animal activity, vegetation type and camera type (Caughley et al., 1976; Chrétien et al., 2015; Chrétien et al., 2016; Patterson et al., 2015; Ransom, 2012; Schlossberg et al., 2016; Zabransky et al., 2016). Two types of camera are most typically used: those that use the Red Green Blue colour model (RGB) and thermal infrared (TIR) devices. RGB cameras acquire images in the light spectrum visible to humans and can be found on most consumer drones. They are often more affordable and may have a higher resolution than TIR cameras (Wich and Koh, 2018). TIR cameras capture infrared radiation which is emitted as heat from different sources of energy as well as endothermic organisms (Vollmer and Möllmann, 2010). This makes them useful for detecting poachers who generally operate at night to reduce the risk of detection (Mulero-Pázmány et al., 2014). TIR cameras have been used for decades to remotely sense wildlife and, with drones, the focus has been to survey large terrestrial as well as marine mammals (Chrétien et al., 2016, 2015; Christiansen et al., 2014; Seymour et al., 2017; Wride and Baker, 1977). In recent years, algorithms have been developed to improve the detection of animals in TIR camera footage and made automatic detection possible (Burke et al., 2018a, 2018b; Christiansen et al., 2014; Longmore et al., 2017; Seymour et al., 2017). There are no studies that have examined the detection probabilities of poachers by RGB and TIR imaging cameras.

In this study we investigate the factors that determine the detection probability of people (subjects) in a miombo woodland in Tanzania. We conducted an experiment in which a drone with RGB and TIR imaging cameras was flown over a group of test subjects to determine which of the following variables influenced detection probability: camera type (RGB or TIR), canopy cover, subjects distance from image centreline, contrast between subject and background and the altitude of the drone. Contrasts between subjects and the background were controlled through use of differently coloured t-shirts. We hypothesized that the probability of detection is negatively affected by a dense canopy cover, a larger distance from the image centreline and higher altitude for both RGB and TIR cameras. In addition, we hypothesized that a larger contrast between the subject and background increases the probability of detection for RGB cameras and that detection will be better with the TIR camera during low light conditions.

2. Methods

2.1. Study area

The study was conducted at the Issa study site (−5.50, 30.56) in the western part of Tanzania. This location lies at 1500 meters (m) above sea level and the dominant vegetation type is miombo woodland (dominated by the genera: *Brachystegia* and *Julbernardia*) (Piel et al., 2015). A list with the 10 most common genera with Diameter at Breast Height (DBH) larger than 10 cm can be found in Appendix A. The data were collected in March 2017, which coincides with the end of the rainy season, when the vegetation is green and dense across the region.

2.2. Drone and cameras

We used a multicopter consisting of a DJI F550 frame with a Pixhawk flight controller. The drone carried two cameras: 1) a 16 MP RGB Survey 2 camera (Mapir, 2016a) with a field of view (FOV) of 82° which was triggered by the flight controller to take an image at 10 m intervals, 2) a ThermalCapture v1.0 TIR camera with a TAU 640 core with a FOV of 45° (TeAx Technology, 2018). The RGB camera was set at ISO 100 and a shutter speed of 1/250. The TIR camera continuously recorded video with automatic settings. All flights were conducted by one of the authors (SW).

2.3. Flight path

Drone flight paths (Appendix B) were created using Mission Planner software (ArduPilot Dev Team, 2017) and uploaded to the Pixhawk flight controller. Take-offs and landings were conducted in loiter mode whereas auto mode was used for the flight pattern. The flight pattern consists of three parallel rows with a length of 70 m each and a connection section of 30 m in length between each row. The descent (dotted line) leads the drone back to its take-off location (Appendix B, Black Square). The flight pattern was performed twice at two different altitudes (70 m and 100 m), providing six rows per flight. The upper altitude of 100 m was chosen as it was close to the usual operation altitude of fixed wing drones while still staying within the legal boundaries of 122 m (400 ft.) (Tanzania Civil Aviation Authority, 2017). The lower altitude of 70 m was chosen as the lowest recommended altitude for safe operation of fixed wing drones and the 70–100 m range was considered suitable for this type of drone. The average flight duration during the data collection was approximately 6 min at a ground speed of 4–5 m/s. We set up two flight areas at different locations to increase the variation in the canopy density and distance from midline data (see Sections 2.6 & 2.8). Both areas had the same flight pattern as can be seen in Appendix B. A total of seven flights were conducted: four in flight area 1 and three in flight area 2. A dawn flight (7:30 am) was conducted in each area, followed by a second flight at dusk on the same day (7:00 pm). These times were chosen to improve the image quality of the TIR images, as lower environmental temperatures create a greater contrast between a person and their surroundings. However, low light levels during several of these flights meant that the RGB camera was unable to produce sufficiently exposed images.

2.4. Location

We selected 24 locations within each flight area and then randomly assigned each test subject to one of them. The locations were chosen for visual criteria on-site to create an equal spatial distribution of locations in the area and with equal frequencies of dense and less dense canopy covers. GPS coordinates of the locations were recorded with the MobileMapper 20 (MM20) model by Spectra Precision. The MM20 has an accuracy of < 2 m in real-time (Trimb et al., 2013).

2.5. Test subjects and t-shirt colours

A group of 10–20 voluntary subjects (varying per flight due to availability) were positioned within the flight area for each of the flights. Each subject wore a standard red, green or blue t-shirt to create a controlled contrast with the background. Each subject wore the same t-shirt and was positioned at the same location for each flight. The test subjects were required to stay at their assigned locations during the flights. A single subject was assigned to each location instead of grouping the subject to increase the statistical power.

2.6. Canopy cover

After the selection of the locations, the canopy densities of the locations were measured by photographing the canopy and calculating the canopy density in the software CanopyDigi (Goodenough and Goodenough, 2016). CanopyDigi gives a calculated value between 0 (open sky) and 1 (completely covered) for each image. Photos were taken with a 24-mm fixed focal length lens mounted on an APS-C camera body with a 1.6 crop sensor resulting in a FOV of 59°. The camera was set up on a tripod at a height of 1.5 m and aligned horizontally using a level. Goodenough and Goodenough (2012) recommend a cloudy sky for best results when photographing the canopy cover. However, this was not always possible and most images were taken with a clear sky and the sun in the frame. This resulted in brighter images which were compensated by adjusting the auto exposure of the camera by −1 stop. This adjustment darkened the images to compensate for the bright sky. The camera was manually focused on the closest branch to ensure sharp images and an aperture of f/16 was used for a sufficient depth of field. ReaConverter Light (ReaSoft Development, 2017) was used to convert the images into the file format required by CanopyDigi (Goodenough and Goodenough, 2012). The threshold values in CanopyDigi were adjusted to deal with images in which the sun was visible in the frame. The thresholds used a range from 45 to 125. The average canopy density was 55%.

2.7. Image processing and analyses

Footage from the two cameras was checked for quality. Any footage taken during take-off, landing or from the connection and transition piece was discarded. We reviewed the footage from the TIR camera in the proprietary ThermoViewer 2.1.2 software (TeAx Technology, 2017). The Non Uniformity Correction (NUC) option was turned on in ThermoViewer, as recommended by the manufacturers. Video footage was converted into 3 to 4 JPG images per row. We converted the RGB camera footage from raw into JPG images using the MAPIR plugin (Mapir, 2016b) for the Fiji software (Schindelin et al., 2012). RGB images were then downscaled to the same resolution as the TIR images (701 × 512) with the Exiftool software (Harvey, 2017). This allows for a universal comparison of the two image types, independent of resolution quality.

The images were analysed separately by three independent analysts, none of whom had previous experience in detecting human subjects in aerial images and who all received the exact same images. Images were provided to the analysts in a random order. In avoiding the sequential showing of all images from one row, analysts could not apply their knowledge of locations from previous images to detect the subjects. The plugin in Cell Count (De Vos, 2010) for the ImageJ 1.8.0 software (Rueden et al., 2017) was used to annotate detected subjects in the images.

The images are not georeferenced and the subjects are identified by their relative location to each other and to landmarks, and the colour of their t-shirts (Appendix C). The results of images from the same row were summarized, thereby simulating a tracking motion in moving images. The multiple angles simulate a tracking motion of a subject in the frame. The tracking enhances the probability of detection because of the multiple camera angles (Gonzalez et al., 2016).

2.8. Calculating the distance to the centreline of the image

We calculated the distance from each subject to the centreline using QGIS 2.18 (Quantum GIS Development Team, 2017). The calculation of the distances used the GPX track as centreline and the shortest distance to each location was calculated with the distance matrix tool.

Table 1
Overview of the tested variables with description.

No	Variable type		Variable	Definition
Response variable				
0	Binary		Detected	Detected = 1; undetected = 0
Predictor variable				
1	Continuous	Fixed	*Canopy density*	Canopy density between 0 and 1
2	Continuous	Fixed	*Distance*	Distance from centreline (m)
3	Binary	Fixed	*Altitude*	70 m = 0; 100 m = 1
4	Nominal	Fixed	*Colour*	White/TIR = 0; red = 1; blue = 2; green = 3
5	Binomial	Fixed	*Time of day*	Dusk = 0; dawn = 1
6	Nominal	Fixed	*Analyst*	Analyst 1, 2, 3
Hierarchical variable				
7	Nominal	Random	Flight number	Identification number of flight

2.9. Statistical analysis

All analyses were carried out using the lme4, glm2 and MuMIn packages in R v3.4.1 (Bates et al., 2017; R Core Team, 2017). We chose a multilevel model approach to accommodate random effects, repeated measurements and crossed data (Field et al., 2012; Grueber et al., 2011; Qian et al., 2010). Following the approach suggested by Grueber et al. (2011), entries with missing data were excluded from the analysis (18 of 2712 entries were excluded). We used a general linear model for the data from the RGB camera as described below. All responses were binary (detection (1)/no-detection (0)) and thus a logit link function was used for all analyses. The variables used in the code for the global data models can be seen in Table 1.

Continuous variables were group-centred. Two separate base data models were created for the TIR images and RGB images. In the TIR base data model, the variable colour was not included since the TIR images only display in black and white. We tested the variable flight area as random intercept but it did not provide an improvement in either models and we excluded the variable in the further analysis. The inclusion of Flight Number as a random intercept significantly improved the TIR data model. However, random effects did not improve the RGB base data model and so a general linear model was used (using the “glm” function in the “glm2” package: Marschner, 2018). Maximum likelihood was used to perform the model estimation for both data models. Data sub-models were created from the base data models, using the function “dredge” from the “MuMIn” (Bartón, 2017) packages as described by Grueber et al. (2011). This resulted in a total of 64 data sub-models for the RGB images and 32 data sub-models for the TIR images. The Akaike Information Criterion corrected for small sample sizes (AICc) was used to assess the data (sub) models (Akaike, 1998; Grueber et al., 2011). Data models with cut-off values of 2AICc were selected using the “get.model” function from the “MuMIn” packages as shown by Bartón (2017) and Grueber et al. (2011). The final data models above this cut-off point were averaged using the zero method to compare between them and identify the one with the best fit (Nakagawa and Freckleton, 2011). These data models have been ranked by their AICc values and their Akaike weight (lower AICc indicates a better model fit and a higher Akaike weight shows a more parsimonious fit overall) (Patterson et al., 2015). We calculated the confidence intervals (CIs) for the best models and converted the logit scale to odds ratio by exponentiating the estimates and CIs.

The last step was to conduct a Tukey's honestly significant difference (HSD) analysis with the “glht” function from the “multcomp” package (Hothorn et al., 2008; Piepho, 2004) to analyse the differences between individual colours and their effect on the probability of detection.

Table 2
The data model with the best fit for the TIR images include the variables Canopy density ($p < 0.001$), Distance ($p < 0.001$) and Analyst ($p = 0.005$).

Variable	Estimate	95% Confident interval	p
(Intercept)	1.086	0.562, 2.095	0.807
Canopy density	0.081	0.053, 0.123	< 0.001
Distance	0.960	0.951, 0.969	< 0.001
Analyst	0.836	0.739, 0.946	0.005

3. Results

To determine which factors influenced detection probability we fitted models to the TIR and RGB data. The analyses are first presented individually and then compared.

3.1. TIR data model

The best TIR data model was selected from three data models based on the criterion described in Appendix D.1.

The best data model contained the variables *Canopy density*, *Distance* and *Analyst*. The best fitting data model is described in Table 2 in more detail.

The variables *Canopy density* and *Distance* had negative coefficients, which indicates a decrease in the probability of detection with an increase in vegetation density and/or increase in distance from the centreline. The negative coefficient for *Analyst* is irrelevant since analysts were ranked in a random order.

3.2. RGB data model

The best data model for the RGB data included *Canopy density*, *Altitude*, *Colour*, and *Analyst* as can be seen in the model selection (Appendix D.2). All of these variables were significant (Table 3). The variables *Canopy density* and *Altitude* had negative coefficients, which indicates that an increase in the vegetation density and altitude negatively influences the probability of detection. The variable *Colour* also had a significant effect on the probability of detection while the variable *Distance* was not included in the best data model, which indicates it does not affect the probability of detection. As in the TIR model, the negative coefficient for *Analyst* was meaningless.

All variables included in the best fitting RGB data model have a negative coefficient indicating that an increase in *Canopy density* and *Altitude* has a negative effect on the probability of detection. The *Colour* variable was further analysed with a Tukey's HSD post-hoc test to assess which colours were significantly different (Fig. 1). The Tukey's HSD analysis showed that the probability of detection of a green subject (a) was significantly lower than the probability of detection of either a blue or red t-shirt (b) (Fig. 1).

3.3. Comparison

The overall detection probability was higher for TIR (41%) images than for RGB (24%) images (Fig. 2, top left). A two sample *t*-test showed a significant ($p < 0.005$) difference in mean detection probabilities between RGB and TIR images.

The best fitting models were compared for TIR and RGB images. Only *Canopy density* (negative coefficient, see Fig. 2, top right) and *Analyst* were included in both data models. *Distance* (Fig. 2, bottom left) was only included in the TIR data model, whereas *Altitude* (Fig. 2, bottom right) and *Colour* were included in the RGB data model. As previously stated, *Colour* was not included in the TIR base data model.

It is important to note that *Time of Day* was not significant in either data model.

Table 3
The best fitting RGB data model includes Canopy density ($p < 0.001$), Altitude ($p < 0.001$), Colour ($p = 0.012$) and Analyst ($p = 0.013$).

Variable	Estimate	95% Confident interval	p
(Intercept)	1.072	0.547, 2.100	0.840
Canopy density	0.011	0.009, 0.014	< 0.001
Altitude	0.399	0.314, 0.509	< 0.001
Colour	0.733	0.503, 1.066	0.012
Analyst	0.749	0.318, 1.764	0.013

4. Discussion

We aimed to identify factors that have a significant effect on the probability of detection of poachers by drones using two camera types (RGB and TIR). Factors that had a significant effect on the probability of detection by TIR images were canopy density, subject distance from the image centreline and the image analyst, while the RGB camera was significant affected by canopy density, altitude of the drone, the subjects' contrast against the background and the image analyst.

Canopy density had a significant negative influence on detection probability for both cameras. This is in accordance with studies on aerial surveying of animals that have found that vegetation density or habitat type has a significant negative impact on probability of detection (Chrétien et al., 2015; Ransom, 2012; Schlossberg et al., 2016; Zabransky et al., 2016). Our results are also consistent with a study that found that habitat type had a significant impact on detection of caribou (Patterson et al., 2015).

Our study also showed a decrease in detection probability with increasing distance from the image centreline, for TIR images. In contrast, no equivalent effect was found in our RGB analysis or by a previous caribou study (Patterson et al., 2015). The latter used a 50-mm lens on a full-frame camera attached to the drone resulting in a FOV of 40°. On this system, distortion and other effects towards the edges of the frame are minimal and it could thus be expected that no effect would be observed. Our RGB camera had a wide-angle lens with a FOV of 82° and therefore has a greater distortion than a normal lens (Brauer-Burchardt and Voss, 2001). In contrast, the TIR camera we deployed in our study had a narrow FOV of 45°. This runs counter to the suggestion that greater distortion from a wider FOV could explain the significant effect for the TIR but not the RGB camera. We were unable to find any similar reports in literature, however, the impact of the distance from the centreline on the probability of detection is well-known in line-transect surveys (Ridgway, 2010). Other studies have hypothesized that subjects' distance from the centreline further decreases the probability of detection by any increase height of the canopy (Israel, 2011).

The RGB images revealed that detection was strongly influenced by the subjects' colour against the background. A similar effect was found by Patterson et al. (2015) who found that targets with greater contrast against the landscape were more easily detected. Detection is also impeded by greater contrast variation in the image background, as this results in variable contrast of the subject against the background (Abd-Elrahman et al., 2005). Chrétien et al. (2015) found animals with cryptic fur have a lower probability of detection because they blend into their environment. Hence, our findings add to previous studies that have shown that aspects of colour, such as contrast, affect the probability detection using RGB images.

Higher flight altitudes also showed lower detection probabilities for RGB images. One way around this might be to use the full resolution original images. Patterson et al. (2015) flew at a constant altitude of around 690 m with no significant variation in elevation in the study area; and therefore was not able to test for the effect of altitude on the probability of detection. However, our results do suggest that the TIR imaging camera is superior at higher flight elevations for the same number of pixels. This could be important in cases where drones must be flown low or where drone height above ground will vary considerably over an area being investigated.

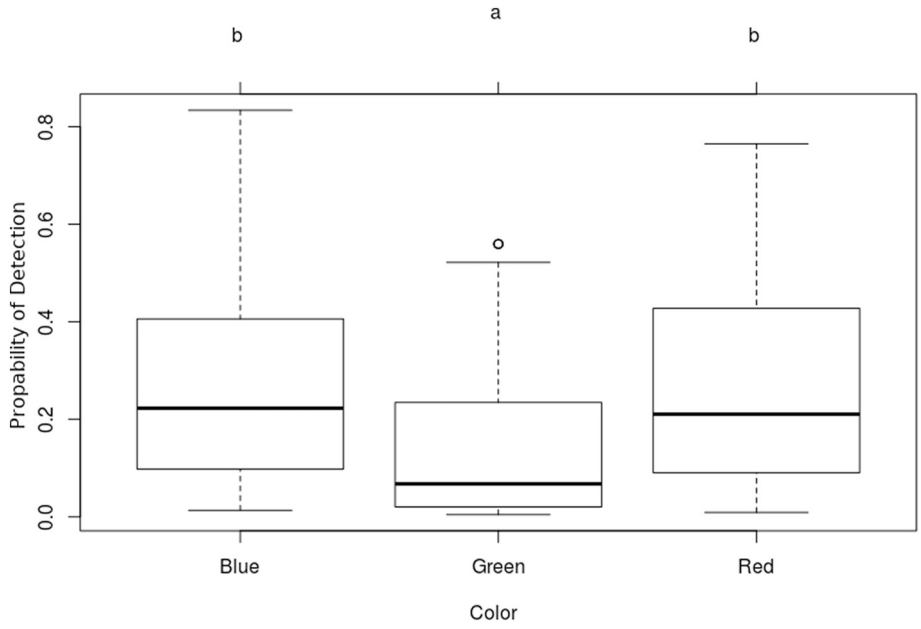

Fig. 1. Box-and-whisker plots that summarize detection probabilities for the three t-shirt colours worn by subjects. The sample sizes are Blue = 324, Green = 192 and Red = 282.

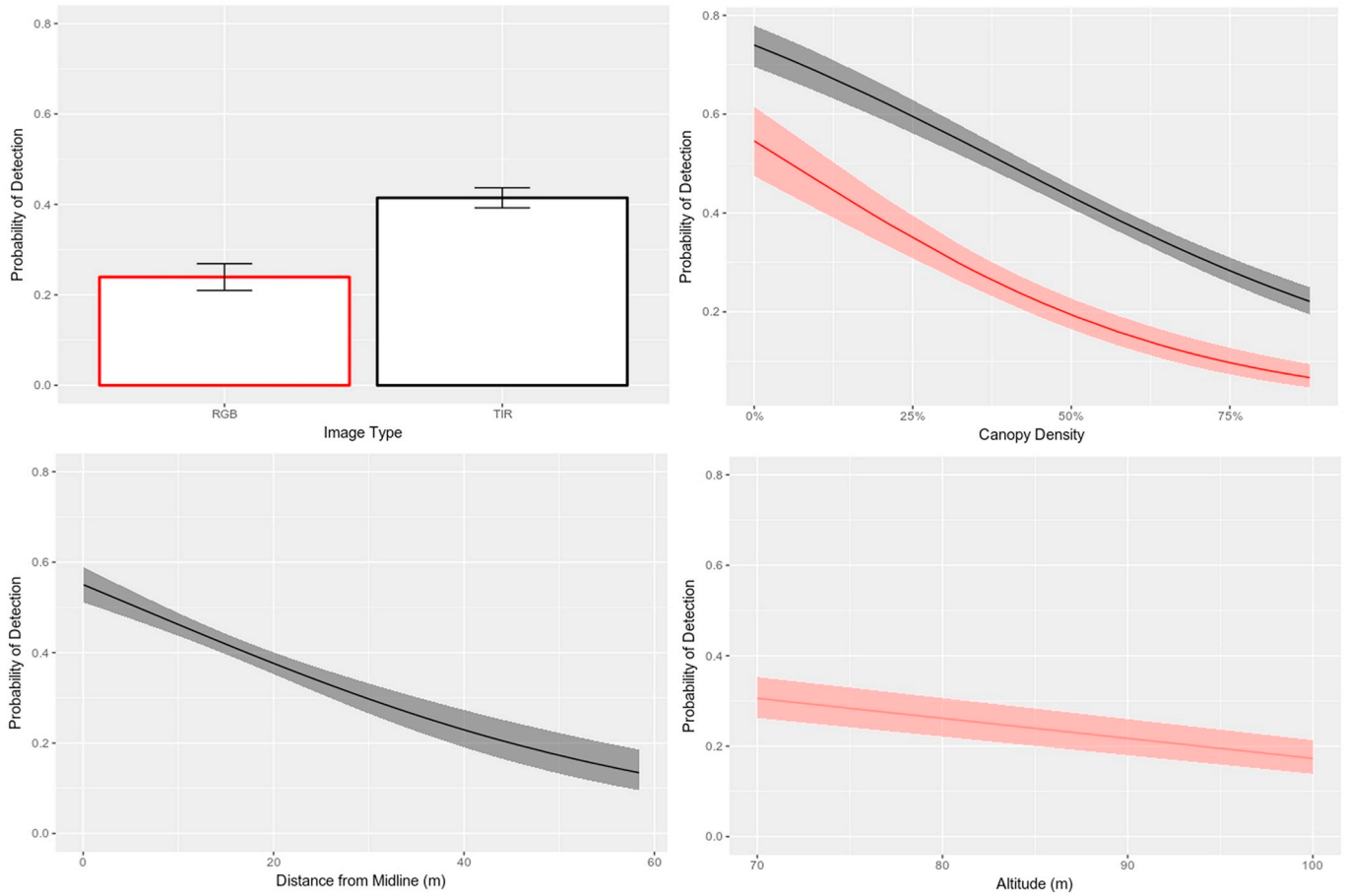

Fig. 2. Comparison between TIR (n = 1896) in black and RGB (n = 798) in red with CIs. Top left shows a bar chart with the probability of detection and associated standard errors. The scatter plot in the top right shows the relationship between the probability of detection and canopy density for each time type, with fitted logit lines. On the bottom left, the scatter plot shows the relationship between the probability of detection and distance from the midline in meters with fitted logit line for TIR. The relationship between the probability of detection and altitude of the drone for RGB is shown in the scatter plot in the bottom right. (For interpretation of the references to colour in this figure legend, the reader is referred to the web version of this article.)

Another significant effect in the data models was the variation in detection probabilities between observers. Patterson et al. (2015) did not find an analyst effect in their study. A possible explanation might be that Patterson et al. (2015) used a controlled procedure for the analysts who were instructed to work through a fixed number of images per day, while the analysts themselves had no previous experience. In our study the analyst effect might be due to the use of three different analysts, with different experience levels.

Time of day was included as factors in the present study for RGB and TIR images, however no significant difference was found. In contrast, Patterson et al. (2015) and Witczuk et al. (2018) found a significant time of day effect. Nonetheless, their flights were performed in a larger time window (7:00–9:30 am and 2:00–3:00 pm), with more targets being detected in the afternoon. Also, their study site was in Labrador, Canada with potentially very different changes in light level between the two flight periods, relative to Tanzania.

The overall probability of detection is relatively low compared to other comparable studies. Chrétien et al. (2016) found a probability of detection (detection rate) of 50% for white-tailed deer using an object-based image analysis and combining TIR and RGB images. Another study surveying hippos found a probability of detection of 85% using TIR images and image analysts (Linchant et al., 2018). One of the main factors causing the difference in probability is the density of the canopy (Witczuk et al., 2018).

It should be noted that some of the differences might be attributed to other camera related factors than only TIR and RGB. Camera settings such as focus, shutter speed and recording format might affect the probability of detection.

An increasing number of research projects are examining the use of drones for ecological conservation and anti-poaching efforts (Chrétien et al., 2015; Christiansen et al., 2014; Christie et al., 2016; Linchant et al., 2015; Martin et al., 2012; Mukwazvure and Magadza, 2014; Mulero-Pázmány et al., 2014; Olivares-Mendez et al., 2015; Patterson et al., 2015; Vermeulen et al., 2013). This is the first study to focus on poacher-detection and the first to explore the factors affecting detection probabilities for TIR imaging. Most other studies that have examined TIR imaging with drones have focused on the automated detection of animals and humans, which is essential to reduce the researcher-hours spent on analysing images and can facilitate near-real time detection of animals/humans in the field (Christiansen et al., 2014; Gonzalez et al., 2016; Longmore et al., 2017; McMillen, 2016; Olivares-Mendez et al., 2015; Seymour et al., 2017). Burke et al. (2018b) applied automatic detection software to the TIR images used in our study. Promising methods for increased detection probabilities lie in the integration and combination of data from multiple sensors such as RGB and TIR cameras by Principal component analysis and Intensity Hue Saturation (Chrétien et al., 2015; Christiansen et al., 2014).

In conclusion, the TIR images allowed for higher detection probability of our experimental poachers than RGB images. This provides a clear advantage against poachers who are trying to hide under vegetation, wear low-contract clothing, or operate at night. However, during the daytime, when temperatures are higher, the RGB performs better than the TIR camera. As expected, poachers hiding under thick vegetation remain undetected with both systems. Distance from the flight midline also influenced detection and should be considered when conducting anti-poaching missions. Potential improvements to detect poachers under trees might be achieved by use of a camera placed at an oblique angle as well as use of machine learning for detection instead of human image analysts.

Acknowledgements

The use of human test subjects for this research was approved by the “University Research Ethics Committee” (UREC) of LJMU, with an approval reference of 17/NSP/008. Flights were performed according to the “LJMU Operations Manual for UAV's” as well as the “Aeronautical Information Circular” (AIC) number 5/17 (Pink 62) of 1 January 2017 and according to the “Tanzania Civil Aviation Regulations” (TCARs).

LH specially thanks Dr. Thomas Grussenmeyer and Charlotte Jense for their time analysing the drone footage and Stefan Thamke from the TeAx Technology company also deserves credit for his support. SW thanks WWF Netherlands for financial support and thanks goes to Tascha Dean, Molly Frost, and John Lamb for proofreading the script. Furthermore, we would like to thank Andy Goodwin and Ian Thomson for support for the drone. Special thanks also go to the students of the 2016/2017 M.Sc. course Wildlife Conservation & UAV Technology as well as to the GMERC (formerly Ugalla Primate Project) staff for their support and patience. The authors would also like to thank: Claire Rigby, Finnoula Taylor, Megan Melia, Jospeh Goode, Derek Dwane, Naomi Jones, Rory Andrews, Anna Starkey, Joseph Phillips, Naomi Davies, Molly Frost, Evie Hyland, Olivia Evans, Jade Musto, Andy Tomlinson, Glory Marie, Mashaka Alimasi, Godfrey Stephano, Mlela Juma, Hussein Juma, Baruana Juma, Abdallah Said, Roda Dominick and Milka Hyamubi. Finally, thanks to Dr. Bryan Pijanowski of Purdue University for the video footage of the data collection.

Declaration of interest

We wish to confirm that there are no known conflicts of interest associated with this publication and there has been no significant financial support for this work that could have influenced its outcome.

Appendix A. 10 Most common genera with DBH larger than 10 cm

Monopetalanthus (13.1%)
Brachystegia (9.8%)
Julbernardia (7.6%)
Baikiaea (4.5%)
Xylopia (2.9%)
Newtonia (2.5%)
Magnistipula (1.8%)
Garcinia (1.6%)
Lindackeria (1.6%)
Syzygium (1.5%)
Percentages relate to the total number of 3200 genera found at the study site.

Appendix B. Flight pattern

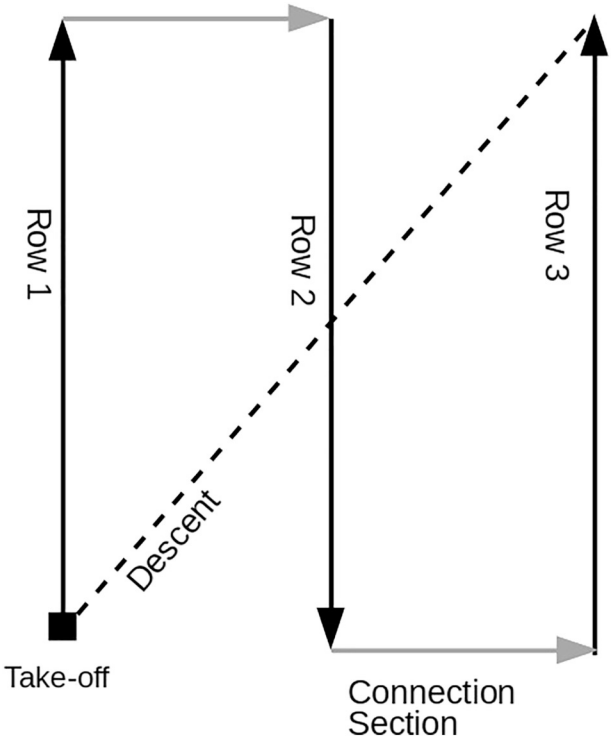

Flight pattern of the drone. Each row is 70 m in length and the connection sections are 30 m long. The decent leads the drone back to the take-off area.

Appendix C. Comparison between RGB and TIR images

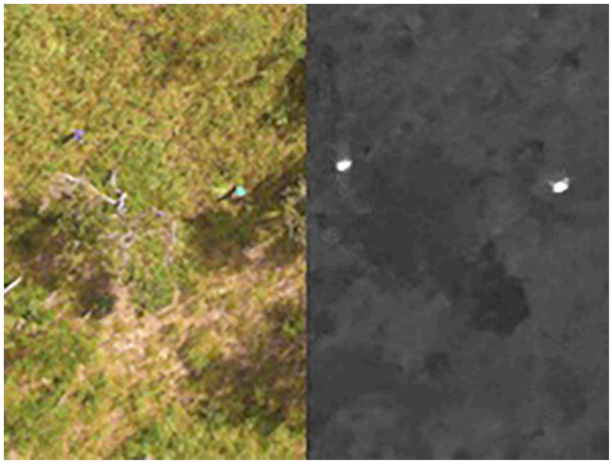

Comparison between RGB images on the left and TIR on right. Both images show the same area, at the same resolution with two people visible.

Appendix D. Model selection

D.1. TIR model selection

Table D.1
A summary of the three selected data models under the AICc criterion (from 32 data sub models) for the detection of subjects using a TIR imaging camera. The best data model includes Canopy density, Distance and Analyst.

Data model name	Df	LogLik	AICc	Delta	Weight
Canopy density + Distance + Analyst	5	−1117.35	2244.72	0.00	0.50
Canopy density + Distance + Time of Day + Analyst	6	−1116.84	2245.72	1.00	0.31
Canopy density + Time of Day + Altitude + Analyst	6	−1117.31	2246.66	1.94	0.19

D.2. RGB model selection

Table D.2
A summary of the top three data models that were selected under the 2AICc criteria (from 64 data sub-models) for the RGB camera. Canopy density, Altitude, Colour and Analyst are included in the best data model.

Data model name	Df	LogLik	AICc	Delta	Weight
Canopy density + Altitude + Colour + Analyst	5	−352.23	714.53	0.00	0.54
Canopy density + Altitude + Colour + Time of Day + Analyst	6	−352.02	716.15	1.62	0.24
Canopy density + Distance + Altitude + Colour + Analyst	6	−352.10	716.31	1.78	0.22

References

Abd-Elrahman, A., Pearlstine, L., Percival, F., 2005. Development of pattern recognition algorithm for automatic bird detection from unmanned aerial vehicle imagery. Surv. Land Inf. Sci. 65, 37.

Air Shepherd, 2017. Home - Air Shepherd [WWW Document]. URL http://airshepherd.org/ (accessed 4.6.17).

Akaike, H., 1998. Information theory and an extension of the maximum likelihood principle, in: Selected Papers of Hirotugu Akaike. Springer, pp. 199–213.

ArduPilot Dev Team, 2017. Misson Planner. (ArduPilot).

Baggaley, K., 2017. Drones are setting their sights on wildlife | Popular Science [WWW Document]. URL http://www.popsci.com/drones-wildlife-biology-animal-research (accessed 8.24.17).

Balazs, E., 2016. From poaching to financing terrorism: thoughts on poaching endangering society. JE-Eur Crim L 190.

Bartón, K., 2017. Multi-model Inference. R Package Version 1.40. 0. 2017.

Bates, D., Maechler, M., Bolker, B., Walker, S., Christensen, R.H.B., Singmann, H., Dai, B., Grothendieck, G., Green, P., 2017. lme4: Linear Mixed-Effects Models using "Eigen" and S4.

Becker, M., McRobb, R., Watson, F., Droge, E., Kanyembo, B., Murdoch, J., Kakumbi, C., 2013. Evaluating wire-snare poaching trends and the impacts of by-catch on elephants and large carnivores. Biol. Conserv. 158, 26–36.

Brauer-Burchardt, C., Voss, K., 2001. A new algorithm to correct fish-eye-and strong wide-angle-lens-distortion from single images, in: Image Processing, 2001. In: Proceedings. 2001 International Conference on. IEEE, pp. 225–228.

Burke, C., Rashman, M., Wich, S., Symons, A., Theron, C., Longmore, S., 2018a. Optimising observing strategies for monitoring warm-blooded animal species using UAV-mounted thermal infrared cameras. - International J. Remote Sens. (in press).

Burke, C., Rashman, M.R., McAgree, O., Hambrecht, L., Longmore, S.N., Piel, A.K., Wich, S.A., 2018b. Addressing Environmental and Atmospheric Challenges for Capturing High-precision Thermal Infrared Data in the Field of Astro-ecology, in: Astronomical Telescopes + Instrumentation. Presented at the SPIE, Austin, Texas, US (in press).

Caughley, G., Sinclair, R., Scott-Kemmis, D., 1976. Experiments in aerial survey. J. Wildl. Manag. 290–300.

Chapron, G., Miquelle, D.G., Lambert, A., Goodrich, J.M., Legendre, S., Clobert, J., 2008. The impact on tigers of poaching versus prey depletion. J. Appl. Ecol. 45, 1667–1674.

Chrétien, L.P., Théau, J., Ménard, P., 2015. Wildlife multispecies remote sensing using visible and thermal infrared imagery acquired from an unmanned aerial vehicle (UAV). Int. Arch. Photogramm. Remote Sens. Spat. Inf. Sci. 40, 241.

Chrétien, L.P., Théau, J., Ménard, P., 2016. Visible and thermal infrared remote sensing for the detection of white-tailed deer using an unmanned aerial system. Wildl. Soc. Bull. 40, 181–191.

Christiansen, P., Steen, K.A., Jørgensen, R.N., Karstoft, H., 2014. Automated detection and recognition of wildlife using thermal cameras. Sensors 14, 13778–13793.

Christie, K.S., Gilbert, S.L., Brown, C.L., Hatfield, M., Hanson, L., 2016. Unmanned aircraft systems in wildlife research: current and future applications of a transformative technology. Front. Ecol. Environ. 14, 241–251.

De Vos, K., 2010. Cell Counter Plugin for ImageJ.

Dinerstein, E., Olson, D., Joshi, A., Vynne, C., Burgess, N.D., Wikramanayake, E., Hahn, N., Palminteri, S., Hedao, P., Noss, R., Hansen, M., Locke, H., Ellis, E.C., Jones, B., Barber, C.V., Hayes, R., Kormos, C., Martin, V., Crist, E., Sechrest, W., Price, L., Baillie, J.E.M., Weeden, D., Suckling, K., Davis, C., Sizer, N., Moore, R., Thau, D., Birch, T., Potapov, P., Turubanova, S., Tyukavina, A., de Souza, N., Pintea, L., Brito, J.C., Llewellyn, O.A., Miller, A.G., Patzelt, A., Ghazanfar, S.A., Timberlake, J., Klöser, H., Shennan-Farpón, Y., Kindt, R., Lillesø, J.-P.B., van Breugel, P., Graudal, L., Voge, M., Al-Shammari, K.F., Saleem, M., 2017. An ecoregion-based approach to protecting half the terrestrial realm. BioScience 67, 534–545. https://doi.org/10.1093/biosci/bix014.

Field, A.P., Miles, J., Field, Z., 2012. Multilevel linear models, in: Discovering Statistics Using R. Sage publications, London; Thousand Oaks, Calif, pp. 855–909.

Gonzalez, L.F., Montes, G.A., Puig, E., Johnson, S., Mengersen, K., Gaston, K.J., 2016. Unmanned Aerial Vehicles (UAVs) and artificial intelligence revolutionizing wildlife monitoring and conservation. Sensors 16, 97.

Goodenough, A.E., Goodenough, A.S., 2012. Development of a rapid and precise method of digital image analysis to quantify canopy density and structural complexity. ISRN Ecol. 2012.

Goodenough, Anne, Goodenough, Andrew, 2016. CanopyDigi.

Grueber, C.E., Nakagawa, S., Laws, R.J., Jamieson, I.G., 2011. Multimodel inference in ecology and evolution: challenges and solutions: multimodel inference. J. Evol. Biol. 24, 699–711. https://doi.org/10.1111/j.1420-9101.2010.02210.x.

Harvey, P., 2017. ExifTool: Read, Write and Edit Meta Information. Softw, Package Available. https://www.sno.phy.queensu.ca/~phil/exiftool/.

Hodgson, J.C., Mott, R., Baylis, S.M., Pham, T.T., Wotherspoon, S., Kilpatrick, A.D., Raja Segaran, R., Reid, I., Terauds, A., Koh, L.P., 2018. Drones count wildlife more accurately and precisely than humans. Methods Ecol. Evol. 9, 1160–1167.

Hothorn, T., Bretz, F., Westfall, P., 2008. Simultaneous inference in general parametric models. Biom. J. 50, 346–363.

Israel, M., 2011. A UAV-based roe deer fawn detection system. Int. Arch. Photogramm. Remote Sens. 38, 1–5.

Kakaes, K., Greenwood, F., Lippincott, M., Dosemagen, S., Meier, P., Wich, S., 2015. Drones and Aerial Observation: New Technologies for Property Rights, Human Rights, and Global Development. New America, Washington, DC, USA, Tech. Rep.

Koh, L.P., Wich, S.A., 2012. Dawn of drone ecology: low-cost autonomous aerial vehicles for conservation. Trop. Conserv. Sci. 5, 121–132.

Lawson, K., Vines, A., 2014. Global Impacts of the Illegal Wildlife Trade: The Costs of Crime, Insecurity and Institutional Erosion. (Chatham House).

Liberg, O., Chapron, G., Wabakken, P., Pedersen, H.C., Hobbs, N.T., Sand, H., 2012. Shoot, shovel and shut up: cryptic poaching slows restoration of a large carnivore in Europe. Proc. R. Soc. B 279, 910–915.

Linchant, J., Lisein, J., Semeki, J., Lejeune, P., Vermeulen, C., 2015. Are unmanned aircraft systems (UASs) the future of wildlife monitoring? A review of accomplishments and challenges. Mammal Rev. 45, 239–252.

Linchant, J., Lhoest, S., Quevauvillers, S., Lejeune, P., Vermeulen, C., Ngabinzeke, J.S., Belanganayi, B.L., Delvingt, W. and Bouché, P., 2018. UAS imagery reveals new survey opportunities for counting hippos. PLoS One, 13(11), p.e0206413.

Longmore, S.N., Collins, R.P., Pfeifer, S., Fox, S.E., Mulero-Pázmány, M., Bezombes, F., Goodwin, A., De Juan Ovelar, M., Knapen, J.H., Wich, S.A., 2017. Adapting astronomical source detection software to help detect animals in thermal images obtained by unmanned aerial systems. Int. J. Remote Sens. 38, 2623–2638.

Lunstrum, E., 2014. Green militarization: anti-poaching efforts and the spatial contours of Kruger National Park. Ann. Assoc. Am. Geogr. 104, 816–832.

Mapir, C., 2016a. Survey2 Cameras [WWW Document]. MAPIR CAMERA. URL https://www.mapir.camera/collections/survey2 (accessed 5.29.18).

Mapir, C., 2016b. Pre-Process Survey2 Images in Fiji with MAPIR Plugin.

Marschner, I., 2018. glm2: Fitting Generalized Linear Models.
Martin, J., Edwards, H.H., Burgess, M.A., Percival, H.F., Fagan, D.E., Gardner, B.E., Ortega-Ortiz, J.G., Ifju, P.G., Evers, B.S., Rambo, T.J., 2012. Estimating distribution of hidden objects with drones: from tennis balls to manatees. PLoS One 7, e38882.
McMillen, D., 2016. Investigating Limitations of SURF Approach for Thermal Imaging Analysis and Mapping.
Mukwazvure, A., Magadza, T.B., 2014. A survey on anti-poaching strategies. Unspecified 3.
Mulero-Pázmány, M., Stolper, R., Van Essen, L.D., Negro, J.J., Sassen, T., 2014. Remotely piloted aircraft systems as a rhinoceros anti-poaching tool in Africa. PLoS One 9, e83873.
Naidoo, R., Fisher, B., Manica, A., Balmford, A., 2016. Estimating economic losses to tourism in Africa from the illegal killing of elephants. Nat. Commun. 7, 13379. https://doi.org/10.1038/ncomms13379.
Nakagawa, S., Freckleton, R.P., 2011. Model averaging, missing data and multiple imputation: a case study for behavioural ecology. Behav. Ecol. Sociobiol. 65, 103–116.
Olivares-Mendez, M.A., Fu, C., Ludivig, P., Bissyandé, T.F., Kannan, S., Zurad, M., Annaiyan, A., Voos, H., Campoy, P., 2015. Towards an autonomous vision-based unmanned aerial system against wildlife poachers. Sensors 15, 31362–31391.
Parveen, N., 2016. British pilot in Tanzania "manoeuvred to save colleague before death." (The Guardian).
Patterson, C., Koski, W., Pace, P., McLuckie, B., Bird, D.M., 2015. Evaluation of an unmanned aircraft system for detecting surrogate caribou targets in Labrador. J. Unmanned Veh. Syst. 4, 53–69.
Piel, A.K., Lenoel, A., Johnson, C., Stewart, F.A., 2015. Deterring poaching in western Tanzania: the presence of wildlife researchers. Glob. Ecol. Conserv. 3, 188–199.
Piepho, H.-P., 2004. An algorithm for a letter-based representation of all-pairwise comparisons. J. Comput. Graph. Stat. 13, 456–466.
Qian, S.S., Cuffney, T.F., Alameddine, I., McMahon, G., Reckhow, K.H., 2010. On the application of multilevel modeling in environmental and ecological studies. Ecology 91, 355–361.
Quantum GIS Development Team, 2017. Quantum GIS Geographic Information System. (Open Source Geospatial Foundation Project).
R Core Team, 2017. R: A Language and Environment for Statistical Computing. R Foundation for Statistical Computing, Vienna, Austria.
Ransom, J.I., 2012. Detection probability in aerial surveys of feral horses. J. Wildl. Manag. 76, 299–307.
ReaSoft Development, 2017. reaConverter - batch image converter that makes it easy to work on millions of files and folders in a single operation.
Ridgway, M.S., 2010. Line transect distance sampling in aerial surveys for double-crested cormorants in coastal regions of Lake Huron. J. Gt. Lakes Res. 36, 403–410.
Rueden, C.T., Schindelin, J., Hiner, M.C., DeZonia, B.E., Walter, A.E., Arena, E.T., Eliceiri, K.W., 2017. ImageJ2: ImageJ for the next generation of scientific image data. BMC Bioinf. 18, 529.
Schindelin, J., Arganda-Carreras, I., Frise, E., Kaynig, V., Longair, M., Pietzsch, T., Preibisch, S., Rueden, C., Saalfeld, S., Schmid, B., 2012. Fiji: an open-source platform for biological-image analysis. Nat. Methods 9, 676.
Schlossberg, S., Chase, M.J., Griffin, C.R., 2016. Testing the accuracy of aerial surveys for large mammals: an experiment with African savanna elephants (Loxodonta africana). PLoS One 11, e0164904.
Seymour, A.C., Dale, J., Hammill, M., Halpin, P.N., Johnston, D.W., 2017. Automated detection and enumeration of marine wildlife using unmanned aircraft systems (UAS) and thermal imagery. Sci. Rep. 7, 45127.
Smart Parks, 2018. Track Record SmartParks [WWW Document]. Smartparks Found. URL https://www.smartparks.org/track-record/ (accessed 5.25.18).
Tanzania Civil Aviation Authority, 2017. AIC 5/17 (pink 62) 1 JAN 2017 - Unmanned Aircraft Systems, 5/17.
TeAx Technology, 2017. ThermoViewer | ThermalCapture - Thermal Imaging Technology.
TeAx Technology, 2018. Flir Tau 2 640 [WWW Document]. URL http://thermalcapture.com/flir-tau-2-640/ (accessed 5.12.18).
Trimb, le Navigation Limited, Trimb, 2013. MobileMapper 20 - Getting Started Guide.
United Nations Office on Drugs and Crime, 2016. World Wildlife Crime Report: Trafficking in Protected Species, 2016, United Nations Publication. United Nations, New York.
Vermeulen, C., Lejeune, P., Lisein, J., Sawadogo, P., Bouché, P., 2013. Unmanned aerial survey of elephants. PLoS One 8, e54700.
Vollmer, M., Möllmann, K.-P., 2010. Infrared Thermal Imaging: Fundamentals, Research and Applications. John Wiley & Sons.
Wich, S.A., Koh, L.P., 2018. Conservation Drones: Mapping and Monitoring Biodiversity. Oxford University Press.
Witczuk, J., Pagacz, S., Zmarz, A., Cypel, M., 2018. Exploring the feasibility of unmanned aerial vehicles and thermal imaging for ungulate surveys in forests-preliminary results. Int. J. Remote Sens. 39 (15–16), 5504–5521.
World Bank, 2018. Tools and Resources to Combat Illegal Wildlife Trade.
Wride, M.C., Baker, K., 1977. Thermal Imagery for Census of Ungulates. (NASA).
Zabransky, C.J., Hewitt, D.G., Deyoung, R.W., Gray, S.S., Richardson, C., Litt, A.R., Deyoung, C.A., 2016. A detection probability model for aerial surveys of mule deer. J. Wildl. Manag. 80, 1379–1389.

Glossary

Altitude: The altitude of the drone measured from the take-off point.
Analyst: Person who reviewed each image from the drone and marks every person detected in the images.
Canopy cover: Percentage of canopy covering the location compared to open sky.
Colour: Test subject have been wearing uniform red, green or blue coloured t-shirt to create a controlled contrast against the green vegetation in the background.
Distance: The distance of a test subject to the centreline of an image in meters.
Field of view (FOV): A measurement of a lens in degrees of the area in front of the lens which is been captured.
Probability of detection: The likelihood that an object is been detecting.
Red Green Blue (RGB): Colour model used by most common cameras today.
Time of Day: Variable to compare the influence of dawn and dusk on the probability of detection.
Thermal infrared (TIR): A wave spectrum which is radiated by warm objects.